The use of slow waves to design simple sound absorbing materials

J.-P. Groby, W. Huang, A. Lardeau, and Y. Aurégan

Citation: Journal of Applied Physics **117**, 124903 (2015); doi: 10.1063/1.4915115
View online: http://dx.doi.org/10.1063/1.4915115
View Table of Contents: http://scitation.aip.org/content/aip/journal/jap/117/12?ver=pdfcov
Published by the AIP Publishing

The use of slow waves to design simple sound absorbing materials

J.-P. Groby,[a] W. Huang, A. Lardeau, and Y. Aurégan
Laboratoire d'Acoustique de l'Université du Maine (LAUM), UMR-6613 CNRS, Av. O. Messiaen, 72085 Le Mans, France

(Received 16 September 2014; accepted 5 March 2015; published online 25 March 2015)

We demonstrate that the phenomenon of slow sound propagation associated with its inherent dissipation (dispersion + attenuation) can be efficiently used to design sound absorbing metamaterials. The dispersion relation of the wave propagating in narrow waveguides on one side of which quarter-wavelength resonators are plugged with a square lattice, whose periodicity is smaller than the wavelength, is analyzed. The thermal and viscous losses are accounted for in the modeling. We show that this structure slows down the sound below the bandgap associated with the resonance of quarter-wavelength resonators and dissipates energy. After deriving the effective parameters of both such a narrow waveguide and a periodic arrangement of them, we show that the combination of slow sound together with the dissipation can be efficiently used to design a sound absorbing metamaterial which totally absorbs sound for wavelength much larger than four times the thickness structure. This last claim is supported by experimental results. © *2015 AIP Publishing LLC*.
[http://dx.doi.org/10.1063/1.4915115]

I. INTRODUCTION

Slow sound propagation is currently a growing topic in acoustics because of the direct analogy with electromagnetic induced transparency. This phenomenon appears when an opaque medium exhibits enhanced transmission in a narrow frequency windows along with strong dispersions. This rapid change in transmission leads to strong dispersion giving rise to slow phase or group velocity waves whose frequency is centered on the narrow transmission band.[1] In acoustics, most of theoretical and experimental evidences of slow sound have been achieved by considering sound propagation in pipes with a series of detuned resonators (mostly Helmholtz resonators) separated by a subwavelength distance,[2] tuned or detuned resonators separated by half of the wavelength giving rise to a coupling between the resonators and the Bragg bandgap,[3] in a waveguided sonic crystals,[4] in lined ducts.[5] So far, only a few studies have been focusing on the dissipation (dispersion and attenuation) of slow sound propagation, even if it has been sometimes noticed or discussed.[2,3,6,7] Dissipation was considered as a side effect of an unexpected adverse reaction. The key point of this article is to make use of slow sound propagation, which appears for a broadband frequency below the bandgap associated with resonator's resonance, together with the associated dissipation to design a sound absorbing metamaterial. By sound absorbing metamaterials, we mean a structured material that exhibits strong or total absorption for wavelength in the air much larger than four times the thickness of the structure L when rigidly backed. Effectively, usual sound absorbing materials, mainly foams, suffer from a lack of absorption at low frequencies when compared to their efficiency at higher frequencies. This results in bulky and heavy multilayered structures, which are mainly efficient for frequencies higher than the so-called quarter wavelength resonance of the backed layer in the inertial regime, i.e., $f = c/4L$. The speed of sound in current porous material is usually of the same order of the sound speed in the air in this regime, because it tends asymptotically to $c_{air}/\sqrt{\alpha_\infty}$, where the tortuosity α_∞ is usually around unity for usual sound absorbing porous materials. The interest of slow sound obviously appears because decreasing the speed of sound in the structure at fixed thickness results in a decrease of the first maximum absorption frequency or decreasing the speed of sound in the structure at fixed frequency results in a decrease of the structure thickness. Over the last decades, several solutions have been proposed to design sound absorbing metamaterials: membrane-type metamaterials that exhibit nearly total reflection at an anti-resonance frequency[8] or nearly total absorption due to the flapping motion of asymmetric rigid platelets added to the membrane[9] have been proposed, but their absorption properties are limited in the metamaterial resonance frequency range; metaporous materials that exhibit quite large total absorption frequency band due to the coupling of several resonance phenomena arising from the embedment of resonant inclusions in a porous matrix,[10] possibly coupled with surface irregularities; double porosity materials[11] or, more recently, dead-end porosity materials.[12] This last solution consists in plugging dead-end pores, i.e., quarter-wavelength resonators, on open pores to create dead-end porosity materials. The derived model consists in adding the admittance of the porous material without the so-called dead-end pores with the one of the so-called dead-end pores, resulting in a low frequency domain of validity of the model and difficulties to understand absorption mechanism. Moreover, the manufacturing process (cooling process) involving salt grains and liquid metal does not yet offer the possibility of the full control over the densities and the lengths of the dead-end pores.

[a]Electronic mail: Jean-Philippe.Groby@univ-lemans.fr.

In this article, we analyze a periodic structure composed of a periodic arrangement of narrow slits, on one side of which quarter-wavelength resonators are plugged with a square lattice, whose periodicity is very small compared to the wavelength. After a description of the configuration in Sec. II and solution of the problem in Sec. III, Sec. IV presents the dispersion analysis of the modes traveling in one of this narrow irregularity and Sec. V presents the derivation of the effective parameters together with their domains of validity. Below the band gap associated with the resonance quarter-wavelength resonators, the sound speed inside the narrow irregularities presents the characteristic of slow sound with an associated dissipation. This enable to design a sound absorbing metamaterial possessing absorption peaks for wavelength in the air much larger than the structure thickness as shown in Sec. V and experimentally validated in Sec. VI.

II. DESCRIPTION OF THE CONFIGURATION

A unit cell of the 2D (in reality 3D) scattering problem together with a sketch of one internal face of the narrow irregularity (subsequently named slit) is shown in Fig. 1. Before the addition of the quarter-wavelength resonators, the unit cell is composed of N identical irregularities of width w and height L occupied by a material M^s modeled as a slit, i.e., the viscous and thermal losses at each lateral boundaries are accounted for. When only plane waves propagate in a slit, the equivalent complex and frequency depend densities and bulk modulus are[13]

$$\begin{aligned} K^s &= \frac{\gamma P_0}{1+(\gamma-1)\tanh\left(\frac{w}{2}\sqrt{-\mathrm{i}\rho^a Pr\omega/\eta}\right)\Big/\left(\frac{w}{2}\sqrt{-\mathrm{i}\rho^a Pr\omega/\eta}\right)}, \\ \rho^s &= \frac{\rho^a}{1-\tanh\left(\frac{w}{2}\sqrt{-\mathrm{i}\rho^a\omega/\eta}\right)/\left(\frac{w}{2}\sqrt{-\mathrm{i}\rho^a\omega/\eta}\right)}, \end{aligned} \tag{1}$$

wherein γ is the specific heat ratio, P_0 the atmospheric pressure, Pr the Prandtl number, η the dynamic viscosity, and ρ^a the density of the saturating fluid. The upper and lower flat and mutually parallel boundaries of the structure, whose x_2 coordinates are L and 0, are designated by Γ_L and Γ_0, respectively.

The upper semi-infinite material M^a, i.e., the ambient fluid that occupies Ω^a, and M^s are in a firm contact at the boundaries $\Gamma_{as}^{(n)}$, $\forall n \in \mathcal{N}$, meaning that the pressure and normal velocity are continuous across $\Gamma_{as}^{(n)}$. The thermal losses are neglected on Γ_0 and Γ_L and a Neumann type boundary condition is applied on these boundaries, i.e., the normal velocity vanishes on Γ_0 and Γ_L. The n-th slit is located at $x_1 = d^{(n)}$, which refers to the slit boundary on which a Neumann type boundary condition is applied, i.e., the interface Γ_N.

A periodic set of r in radii quarter-wavelength resonators of length l are plugged on one lateral face of the slit with a square lattice of size a in the x_2–x_3 plane, see Fig. 1. The material M^t that occupies each tube Ω^t is modeled as a circular tube and is in firm contact with M^s through Γ_{st}, i.e., the pressure and normal velocity are continuous across Γ_{st}. When only plane waves propagate in a tube, the equivalent complex and frequency depend densities and bulk modulus are[13]

$$\begin{aligned} K^t &= \frac{\gamma P_0}{1+2(\gamma-1)/\sqrt{-\mathrm{i}\rho^a Pr\omega/\eta}\mathrm{J}_1\left(r\sqrt{-\mathrm{i}\rho^a Pr\omega/\eta}\right)/r\mathrm{J}_0\left(r\sqrt{-\mathrm{i}\rho^a Pr\omega/\eta}\right)}, \\ \rho^t &= \frac{\rho^a}{1-2/\sqrt{-\mathrm{i}\rho^a\omega/\eta}\mathrm{J}_1\left(r\sqrt{-\mathrm{i}\rho^a\omega/\eta}\right)/r\mathrm{J}_0\left(r\sqrt{-\mathrm{i}\rho^a\omega/\eta}\right)}, \end{aligned} \tag{2}$$

wherein J_n is the Bessel function of n-th order. The thermal losses are neglected on Γ_l and a Neumann type boundary condition is applied on these boundaries, i.e., the normal velocity vanishes on Γ_l. The first conditions on Γ_{st} will be reduced to an impedance condition applied on the whole interface Γ_Z in the following, because the considered wavelength is much larger than the dimensions of Γ_{st} and the periodicity of this arrangement a inside the slit. This impedance, which already accounts for the material propagation and losses in the tubes, and for the conditions on Γ_{st} and Γ_l reads as

$$Z^{\pm} = \pm\mathrm{i}Z^t \operatorname{cotan}(k^t l)/\phi^t, \tag{3}$$

wherein $Z^t = \sqrt{\rho^t K^t}$ is the impedance of M^t, k^t is the wavenumber inside the tube, and ϕ^t is the ratio between the area of Γ_{st} over the one of the unit cell, i.e., a surface porosity $\phi^t = \pi r^2/a^2$. The sign $\pm$ depends on whether the tubes are

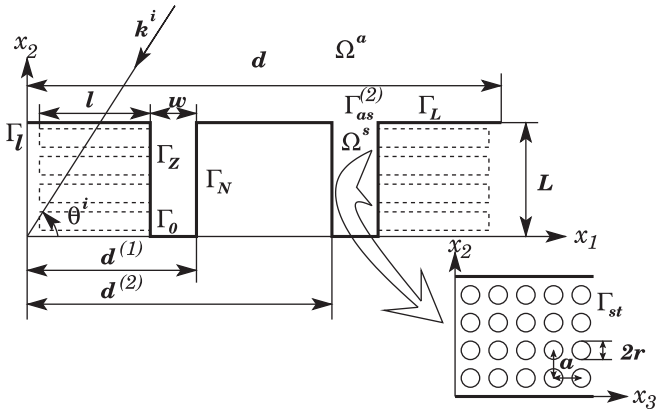

FIG. 1. Example of a d-periodic structure, whose unit cell is composed of 2 slits with quarter-wavelength resonators plugged on one side of them.

plugged on the right (+ sign) or left (– sign) side of the slit. In what follows, only the positive sign will be used and $Z = Z^+$. The problem therefore reduces to a 2D one. The impedance condition does not account for losses on the rigid portion of Γ_Z, i.e., $\Gamma_Z \backslash \Gamma_{st}$, while use of Eq. (1) accounts for losses on a fully rigid boundary. The combination of Eq. (1) and the application of this impedance condition are also valid under the hypothesis of small ϕ^t. This hypothesis is usually accepted when dealing with dissipation in ducts with resonators.[7,14]

The incident wave propagates in Ω^a and is expressed by $p^i(\mathbf{x}) = A^i e^{\mathrm{i}(k_1^i x_1 - k_2^{ai}(x_2 - L))}$, wherein $k_1^i = -k^a \sin\theta^i$, $k_2^{ai} = k^a \cos\theta^i$ and $A^i = A^i(\omega)$ is the signal spectrum.

In each domain Ω^α ($\alpha = a, s, t$), the pressure field fulfills the Helmholtz equation

$$\nabla \cdot \left(\frac{1}{\rho^\alpha} \nabla p^\alpha \right) + \frac{(k^\alpha)^2}{\rho^\alpha} p^\alpha = 0, \tag{4}$$

with the density ρ^α and the wavenumber $k^\alpha = \omega / c^\alpha$, defined as the ratio between the angular frequency ω and the sound speed $c^\alpha = \sqrt{K^\alpha / \rho^\alpha}$.

As the problem is periodic and the excitation is due to a plane wave, each field (X) satisfies the Floquet-Bloch relation

$$X(\mathbf{x} + \mathbf{d}) = X(\mathbf{x}) e^{\mathrm{i}k_1^i d}. \tag{5}$$

Consequently, it suffices to examine the field in the elementary cell of the material to get the fields, via the Floquet relation, in the other cells.

III. SOLUTION OF THE PROBLEM

A. Field representations

Separation of variables, radiation conditions, and Floquet theorem leads to the representations

$$p^a(\mathbf{x}) = \sum_{q \in \mathbb{Z}} [A^i e^{-\mathrm{i}k_{2q}^a (x_2 - L)} \delta_{0q} + R_q e^{\mathrm{i}k_{2q}^a (x_2 - L)}] e^{\mathrm{i}k_{1q}^a x_1}, \forall \mathbf{x} \in \Omega^a, \tag{6}$$

wherein δ_{0q} is the Kronecker symbol, $k_{1q}^a = k_1^i + \frac{2q\pi}{d}$, and $k_{2q}^a = \sqrt{(k^a)^2 - (k_{1q}^a)^2}$, with $\mathrm{Re}(k_{2q}^a) \geq 0$ and $\mathrm{Im}(k_{2q}^a) \geq 0$. The reflection coefficient of the Bloch wave denoted by the subscripts q is R_q.

According to Ref. 15, the pressure field $p^{s(n)}$, admits the pseudo-modal representation, that already accounts for the boundary conditions on Γ_0, Γ_N and Γ_Z:

$$p^{s(n)} = \sum_{m \in \mathbb{N}} A_n \cos\left(k_{1m}^s (x_1 - d^{(n)})\right) \cos\left(k_{2m}^s x_2\right) \forall \mathbf{x} \in \Omega^{s(n)}, \tag{7}$$

wherein A_n are the coefficients of the pseudo modal representation, $k_{2m}^s = \sqrt{(k^s)^2 - (k_{1m}^s)^2}$, with $\mathrm{Re}(k_{2m}^s) \geq 0$ and $\mathrm{Im}(k_{2m}^s) \geq 0$, and k_{1m}^s is the m-th solution of the dispersion relation and satisfies

$$k_{1m}^s \tan\left(k_{1m}^s w\right) = \frac{-\mathrm{i}\omega\rho^s}{Z}. \tag{8}$$

This last equation is solved by use of a Muller's algorithm[16] initiated with the low frequency approximations

$$\tilde{k}_{10}^s = \sqrt{-\mathrm{i}\omega\rho^s w / Z}/w, \quad \text{and}$$
$$\tilde{k}_{1m}^s = m\pi\left(1 + \sqrt{1 - 4\mathrm{i}\omega\rho^s w / Z (m\pi)^2}\right)/2w. \tag{9}$$

These modes are said bi-orthogonal and the bi-orthogonality relation reads as

$$\int_0^w \cos\left(k_{1m}^s x_1\right) \cos\left(k_{1M}^s x_1\right) dx_1 = \delta_{Mm} w \left(1 + \mathrm{sinc}(2k_{1m}^s w)\right)/2 = \delta_{Mm} w N_m. \tag{10}$$

B. The linear system for the solution of R_q

The application of the boundary conditions on each interface $\Gamma_{as}^{(n)}$ leads to two set of coupled equations in terms of $A_m^{(n)}$ and R_q: the continuity of the pressure field is projected on each Bloch mode (making use of the orthogonality of these modes), while the continuity of the normal component of the velocity is projected on the mode of the slit (making use of the bi-orthogonality relation (10)). The combination of these two set of equations leads to the solution either in terms of R_q or in term of A_m, these two solutions being linked one with each other. In particular, the linear system of equations for the solution for R_q, $\forall q \in \mathbb{Z}$, is

$$R_q - \frac{\mathrm{i}\rho^a}{k_{2q}^a} \sum_{Q \in \mathbb{Z}} R_Q \sum_{n \in \mathcal{N}} \sum_{m \in \mathbb{Z}} \frac{k_{2m}^s \phi^{s(n)}}{\rho^s N_m} \tan\left(k_{2m}^s L\right) I_{mq}^{l/r(n)-} I_{mQ}^{l/r(n)+} = A^i \delta_q + A^i \sum_{n \in \mathcal{N}} \sum_{m \in \mathbb{Z}} \frac{\mathrm{i}\rho^a k_{2m}^s \phi^{s(n)}}{k_{2q}^a \rho^s N_m} \tan\left(k_{2m}^s L\right) I_{mq}^{(n)-} I_{mQ}^{(n)+}, \tag{11}$$

where $\phi^{s(n)} = w/d$ is the surface porosity of one slit, such that $\cup_{n \in \mathcal{N}} \phi^{s(n)} = \phi^s$ is the global surface porosity of the structure, and

$$I_{mq}^{(n)\pm} = \frac{e^{\pm \mathrm{i}k_{1q}^a \left(d^{(n)} - \frac{w}{2}\right)}}{2} \left[e^{\mathrm{i}k_{1m}^s \frac{w}{2}} \mathrm{sinc}\left(\left(k_{1m}^s \pm k_{1q}^a\right) \frac{w}{2} \right) + e^{-\mathrm{i}k_{1m}^s \frac{w}{2}} \mathrm{sinc}\left(\left(k_{1m}^s \mp k_{1q}^a\right) \frac{w}{2} \right) \right], \tag{12}$$

when the impedance condition is applied on the right side of the n-th slit and

$$I_{mq}^{(n)\pm} = \frac{e^{\pm ik_{1q}^a\left(d^{(n)}+\frac{w}{2}\right)}}{2}\left[e^{-ik_{1m}^s\frac{w}{2}}\mathrm{sinc}\left(\left(k_{1m}^s \pm k_{1q}^a\right)\frac{w}{2}\right) + e^{ik_{1m}^s\frac{w}{2}}\mathrm{sinc}\left(\left(k_{1m}^s \mp k_{1q}^a\right)\frac{w}{2}\right)\right], \quad (13)$$

when the impedance condition is applied on the left side of the n-th slit.

The system Eq. (14) is solved for each q and each m. The absorption coefficient A is then calculated through

$$A = 1 - \sum_{q\in\mathbb{Z}} \frac{\mathrm{Re}\left(k_{2q}^a\right)}{k_2^a} \| R_q\|^2. \quad (14)$$

IV. ANALYSIS OF THE DISPERSION RELATION IN THE SLITS

The width of the slit, tube dimensions, and the square lattice dimension is fixed at $w = 2$ mm, $r = 2.5$ mm, $l = 40$ mm, and $a = 7$ mm. The surface porosity ϕ^t is 0.4. Figure 2 depicts the real part of solution of the dispersion relation Eq. (8) with and without losses. In this last case, $\rho^s = \rho^t = \rho^a$ and $K^s = K^t = K^a$. The 0-th order mode possesses a cut-off frequency with an infinite branch when $\mathrm{cotan}(k^t l) = \mathrm{cotan}(k^a l) = 0$. This make the higher modes continuously shift down of a value of π/w, which means that these modes change symmetry, from a symmetric to an antisymmetric one, and the opposite. The impedance condition continuously passes from a condition close to a Neumann one at low frequency to a Neumann one at higher frequency through a Dirichlet one at the resonance of the tubes. When losses are introduced, and for small values of w, these modes do not intersect anymore and do not change symmetry. This implicitly means that a Dirac cone is theoretically possible with mode repulsion for particular couple (w, l). These modes are correctly approximated by their low frequency approximation $\tilde{k}_{1m}^s$ given Eq. (9). The real part of k^s is also plotted in Figure 2. Only the fundamental mode $\tilde{k}_{10}^s$ leads to propagative waves.

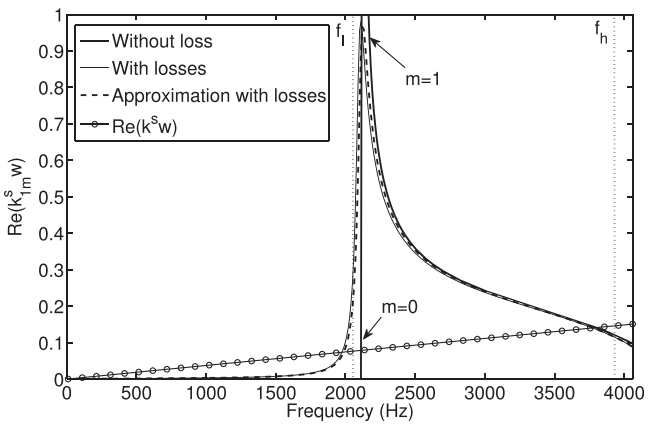

FIG. 2. Real part of $k_{1m}^s w$, without and with losses, as well as $\tilde{k}_{10}^s w$. The real part of $k^s w$ is also plotted, as well as the position of both bounds of the bandgap f_l and f_h.

This fundamental mode is close to a plane mode when propagative, because $\tilde{k}_{10}^s w \ll \pi$. This fact together with the small value of ϕ^t ensure the validity of the combination of Eq. (1) with the application of this impedance condition. The structure possesses a bandgap associated with the resonance of the quarter-wavelength resonators. Because of the losses, the bandgap definition and bounds are not clear. Nevertheless, it corresponds to $\tilde{k}_{10}^s = k^s$, i.e., $\tan k^t l = -k^s w Z^t / Z^s \phi^t$. Assuming all properties of the materials to be frequency independent and real, the low frequency bound corresponds to the first sign change of $\tan(k^t l)$, i.e., $f_l \approx c^t/4l$, while the high frequency bound corresponds to $\tan(k^t l) \approx k^t l - \pi$, i.e., $f_h = 1/(2(l/c^t + wZ^t/c^s Z^s \phi^t))$. When the material properties are frequency dependant, these two frequencies can be determined by the intersection of the real part of the previous expression with f. This leads to $f_l \approx 2080$ Hz and $f_h \approx 3890$ Hz, whose value highlight the difficult determination of the bandgap bounds in case of losses and dispersion. While f_l corresponds to the quarter wavelength frequency of the tubes, f_h also depends on various parameters among which the dimensions and mechanical parameters of the slit. This explain why f_h is that affected when compared to f_l by the flow in duct experiments, for example.[5]

Among the bandgap, a particular feature of the sound wave propagating in the slit is its velocity. Figure 3(a) depicts the sound speed of the wave traveling in the slit, i.e., $\mathrm{Re}(\omega/k_{20}^s)$, its approximation, i.e., $\mathrm{Re}(\omega/\tilde{k}_{20}^s)$, the sound speed of air and the sound speed in the slit in absence of tubes $\mathrm{Re}(c^s) = \mathrm{Re}(\sqrt{\kappa^s/\rho^s})$. Four zones are exhibited: At very low frequency, sound speed vanishes because of the viscous regime; below f_l, the sound speed is smaller than the speed of sound in the air and in the slit in absence of tubes, i.e., subsonic regime; inside the bandgap $[f_l, f_h]$, the sound speed vanishes; above f_h, the sound speed is higher than the air speed of sound, i.e., supersonic regime. Notice that again the bandgap does not seem to have the same bounds as before, because of the losses and dispersion. The supersonic regime was already noticed in Ref. 17 over a small frequency range just after Helmholtz resonance, while the infrasonic regime is to some extend (in the sense that an acoustic wave always propagate in a porous medium with a velocity a little bit smaller than in the air) common in the porous community. Nevertheless, we clearly demonstrate hereafter that this infrasonic regime is not due to a common tortuosity effect. Below f_l, the sound speed possesses a plateau at low frequency and slowly decreases to a value close to zero at f_l. The value of this plateau can be approximated ($k^t l \ll 1$) by the low frequency limit $\mathrm{Re}(c^s/\sqrt{1 + \phi^t l Z^s c^s / w Z^t c^t})$, Figure 3(a). This value is always much smaller than $\mathrm{Re}(c^s)$ if $\phi^t l > w$. Without losses, this limit reduces to $c^a/\sqrt{1 + \phi^t l/w}$, which clearly shows that the speed of sound in the slit is always smaller than c^a and decreases when the ratio $\phi^t l/w$ increases. Focusing on the frequency band below f_l, the group velocity, defined as $v_g^s = \mathrm{Re}(\partial\omega/\partial k_{20}^s)$ is also much lower than the speed of sound in the air and tends to zeros at f_l.

The absorption is related to $\mathrm{Im}(k_{20}^s)$. Figure 3(b) depicts $\mathrm{Im}(k_{20}^s)$ in the slit and its approximation $\mathrm{Im}(\tilde{k}_{20}^s)$. The imaginary part of k_{20}^s is very large inside the bandgap.

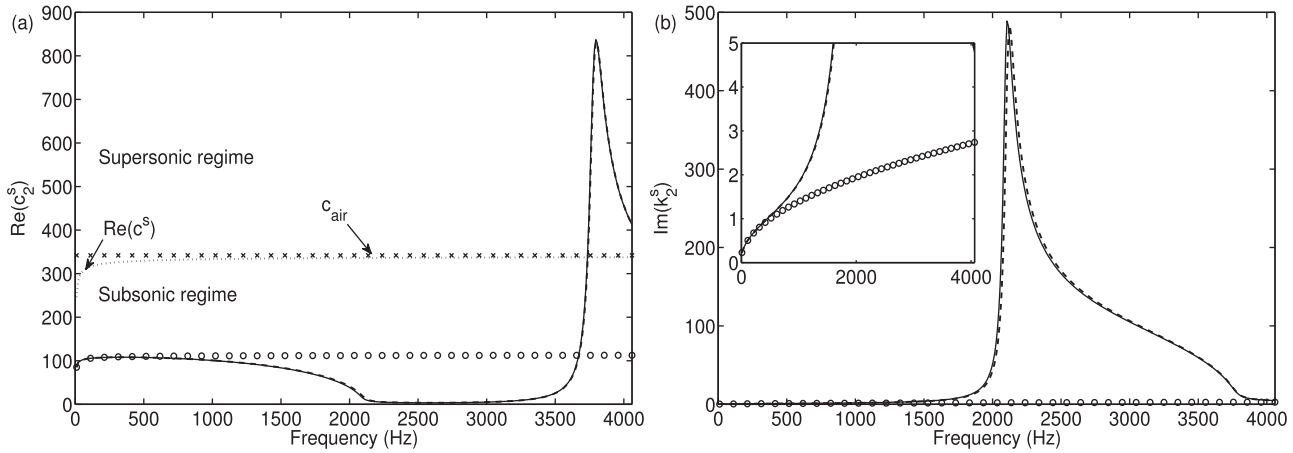

FIG. 3. (a) Real part of c_2^s (—) and of $\tilde{c}_2^s$ (– –), as well as c_{air} (×) and Re(c^s) (· · ·). The asymptotic low frequency limit of c_2^s is also plotted (○). (b) Imaginary part of k_2^s (—) and of $\tilde{k}_2^s$ (– –). The asymptotic low frequency limit of Im(k_2^s) is also plotted (○).

The low frequency limit ($k^t l \ll 1$) of $\mathrm{Im}(\tilde{k}_{20}^s)$ is $\mathrm{Im}(k^s\sqrt{1+\phi^t l Z^s c^s/wZ^t c^t})$, which clearly show that the absorption increases with the ratio $\phi^t l/w$. So, to ensure low sound speed and large attenuation, the ratio $\phi^t l/w$ should be large.

V. DERIVATION OF THE EFFECTIVE PARAMETERS

Assuming the unique propagation of the mode $m=0$ in the slits and $k_{10}^s w \ll 1$, $N_0 \approx 1$. The assumption that the frequency is much lower than the Wood anomaly frequency, which corresponds to $k_{1q}^a = k^a$ when $q=\pm 1$, i.e., when only the specularly reflected wave propagates, is not sufficient to derive effective parameters because of the terms $I_{0q}^{(n)\pm}$ in Eq. (11). To do so, the condition $(k_{10}^s \pm k_{1q}^a)w/2 \gg 1$, $\forall q \neq 0$ should be imposed. This condition ensures that only the term $q=0$ does not vanish and that $I_{00^{(n)\pm}} = 1$. It implicitly means that the position of slits $d^{(n)}$ as well as the side of the slit on which the impedance condition is applied, either on the right or the left of the slit, does not affect the effective parameters. In other words, it means that different structure of different periodicity can have identical effective parameters. This last condition is more restrictive than the first one, because it also ensures that the higher order Bloch modes, which are only related to the arrangement of the slits, do not contribute to the field, while $q\pi/d$ is always very large. This condition is often forgotten by the porous material community, which mainly focuses on the propagation inside the pores, a few on their arrangement, but never on the possible contribution of evanescent waves. Effectively, the macroscopic description of the propagation inside the slit is subjected to $k_1^s w \ll 1$, $k^t r \ll 1$, and $k_{20}^s a \ll 1$. The macroscopic description of the propagation inside the material is also subjected to $(k_1^s \pm k_{1q}^a)w/2 \gg 1$, $\forall q \neq 0$. In the frequency range, where the condition $k_{1q}^a < k^a$ when $q=\pm 1$ is satisfied, but the condition $(k_{10}^s \pm k_{1q}^a)w/2 \gg 1$, $\forall q \neq 0$ is not satisfied, the higher order Bloch modes do not propagate but can contribute significantly to the field and so to the properties of the material. This is due to the large dispersion of k_{10}^s close to the resonance frequency of the resonators, which shifts the sinc function windowing and could make $I_{0q^{(n)\pm}}$ large for $q \neq 0$. The contribution of these evanescent waves, which are localized close to the interface of the material can nevertheless be accounted for through Drude transition layers.[19,20]

When $(k_{10}^s \pm k_{1q}^a)w/2 \gg 1$, $\forall q \neq 0$, the system Eq. (11) reduces to the unique calculation of R_0, which reads as

$$R_0 = A^i \frac{\mathrm{i}\omega\rho^s \cot(k_{20}^s L)/k_{20}^s \phi^s - Z_0/\sin\theta^i}{\mathrm{i}\omega\rho^s \cot(k_{20}^s L)/k_{20}^s \phi^s + Z_0/\sin\theta^i}. \tag{15}$$

A simple identification with the classical formula of the reflection coefficient of a rigidly backed homogeneous slab leads to a surface impedance

$$Z = \mathrm{i}\omega\rho^s \cot(k_{20}^s L)/k_{20}^s \phi^s. \tag{16}$$

This impedance does not depend on the angle of incidence. Sound propagation in each slit depends only on the pressure of air above the slit, and the material is a locally reacting material.[21] Another simple identification leads to $Z_{eff} = \omega\rho^s/\tilde{k}_2^s \phi^s$ and $k_{eff} = \tilde{k}_2^s$, where we make use of Eqs. (3) and (9), the validity of these expressions being ensured. The effective density ($\rho_{eff} = Z_{eff} k_{eff}/\omega$) and bulk modulus ($K_{eff} = \omega Z_{eff}/k_{eff}$) of this locally reacting material would read as $\rho_{eff} = \rho^s/\phi^s, K_{eff} = K^s/\phi^s(1+Z^s\phi^t \tan(k^t l)/Z^t k^s w)$. Nevertheless, these formula are derived accounting for the unique porosity of the slit and not for the porosity of the whole structure. Doing so, the effective density and bulk modulus of this locally reacting material read as

$$\rho_{eff} = \frac{\rho^s\left(1+\phi^t l/w\right)}{\phi^{tot}},$$
$$K_{eff} = \frac{K^s\left(1+\phi^t l/w\right)}{\phi^{tot}\left(1+Z^s\phi^t \tan(k^t l)/Z^t k^s w\right)}, \tag{17}$$

where ϕ^{tot} is the porosity of the whole structure and $\alpha_\infty = (1+\phi^t l/w) = \phi^{tot}/\phi^s$ is a tortuosity-like parameter. In this last case, $\lim_{\omega\to 0} K_{eff} = P_0$, which is the usual value limit of the bulk modulus in the classical porous material representation. These effective parameters are independent on wave

propagation direction and structure thickness. The effective density and bulk modulus in the slits are $\rho^s_{eff} = \rho_{eff}\phi^{tot} = \rho^s(1 + \phi^t l/w)$ and $K^s_{eff} = K_{eff}\phi^{tot}$, i.e., a unusual tortuosity is introduced and the effective bulk modulus is modified. The addition of the periodic set of resonators acts on the thermal losses and introduces an unusual tortuosity, which acts on the density of the slit and not on a mixture of the densities of the slit and of tubes. To be convinced of the influence of the thermal losses, the assumption $k^t l \ll 1$ leads to $K^s_{eff} = K^s(1 + \phi^t l/w)/(1 + \phi^t K^s l/wK^t)$, which only depends on the effective bulk modulus in the tube and the slit and so on the thermal losses.

Let us consider $\mathcal{N} = 1$, and the dimension used in Sec. IV with $d = 42$ mm. This corresponds to a very thin plate ending the quarter wavelength resonator. Figure 4 depicts the normalized real and imaginary part of the effective bulk modulus and density as well as their approximation: normalized by P_0/ϕ^{tot} and by ρ^a/ϕ^{tot} for the material and normalized by P_0 for the material and by ρ^a for the slit. The effective parameters for the materials are only valid till f_l, while the effective parameters for the slit are valid on the whole range of frequency considered. A particular feature of the real part of the effective modulus in the slit is that it becomes negative on the whole frequency of the bandgap associated with the resonance of the resonators. This is in accordance with previous results obtained in case of Helmholtz resonators[17] since the seminal article.[18] A particular feature of the real part of the density is its particularly large value, which is due to a particularly large tortuosity-like effect only acting on the density of the slit. Imaginary part of both effective parameters is in accordance with the passivity condition,[20] with $\mathrm{Im}(K_{eff}) < 0$ and $\mathrm{Im}(\rho_{eff}) > 0$.

Let us remark that the extension to a 3D problem with quarter-wavelength resonators plug on a straight pore is straightforward, by defining the proper porosity and using the proper formulas for the effective parameters for the straight pore.

VI. RESULTS AND DISCUSSION

The infinite sums in Eq. (11) are truncated at M and $Q \pm$. The goal is to design a material that achieves large absorption at low frequency. Low frequency means for a wavelength in the air larger than four times the thickness of the structure, where only one reflected Bloch wave is propagating. The high frequency bound can be approximated by the frequency at which the Wood anomaly happens.[22]

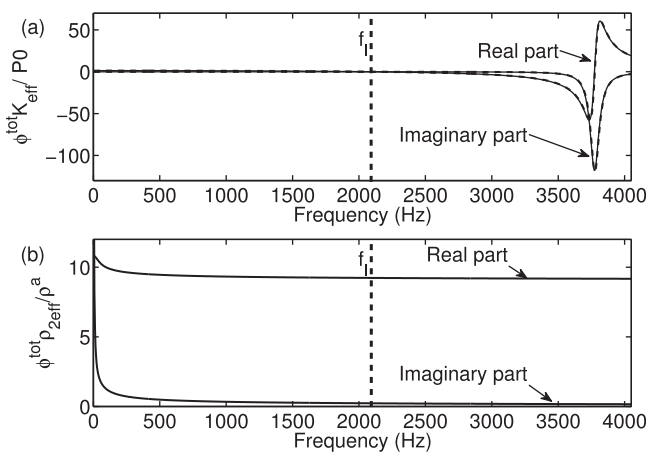

FIG. 4. Normalized real and imaginary part of the effective bulk modulus (a) and density (b) as well as their approximation. Solid curves depict the direct calculation of the effective parameters through k^s_1, while the dashed curves depict their approximated values Eq. (17).

In our case, the large absorption is only associated with the quarter wavelength resonance of the slits. Contrary to the one usually encountered for regular porous material and associated with interference phenomena, this quarter wavelength resonance is a real resonance of the slits. For fixed ratio $\phi l/w$, Figure 3 shows that the sound speed decreases from a plateau, while the attenuation $\mathrm{Im}(k^s_2)$ increases with frequency below the bandgap. This means that the structure possesses an optimum in terms of attenuation-thickness of the structure at the quarter wavelength resonance of the slit when the frequency of the end of the plateau f_{opt} equals $c^s_2/4L$. For the dimensions considered in Sec. IV, $f_{opt} \approx 550$ Hz, which leads to $L \approx 45$ mm. In practice, this length can be smaller. Figure 5(a) depicts the absorption coefficient for $d = 84$ mm, $L = 42$ mm, $N = 2$, with $d^{(1)} = d^{(2)} = 42$ mm (the other dimensions are those of Sec. IV), with the quarter wavelength resonators plugged on the left for the first slit and on the right for the second slit, when $M = 2$ and $Q \pm = 0$, $Q^{\pm} = 22$ as well as the calculation ran with the equivalent parameters derived in Sec. V at normal incidence. It should be noticed that in this case, the equivalent parameters being independent of the slit position and side of the slit on which the impedance condition is applied, the effective parameters reduce to those of $N = 1$ and $d' = 42$ mm. Their validity is ensured till the quarter-wavelength resonance. The calculation performed with the help of the effective parameters is identical (as expected) with the calculation performed when only the terms $Q = 0$ is dominant. While the calculation derived with the effective parameters constitutes a good approximation, the effect of the Drude transition layers[19] is clearly visible around this bound, f_l. Effectively, the required number of Bloch mode is very large at the lower bound of the bandgap. This is explained by the large dispersion of the waves inside the slits around this frequency. The absorption coefficient vanishes inside the bandgap because all the energy is reflected. The structure response possesses absorption peaks which all correspond to resonances of the slits.

The large absorption obtained at 590 Hz is of particular interest. It should be noticed that this peak is not associated with the resonance of the resonators but to a resonance of the slit with a sound velocity reduced because of the presence of the side resonators. In first approximation, the sound speed is reduced by a factor $\sqrt{1 + \phi^t l/w} = \sqrt{\alpha_\infty} \approx 3$. Thus, this material will be efficient at a frequency 3 times smaller than a classical one. This frequency corresponds in practice to a wavelength in the air $\lambda^a = 579.6$ mm, which is 14 times bigger than the thickness of the structure. The higher order quarter wavelength resonances lead to large absorption peak, which concentrates around f_l because the speed of sound is rapidly decreasing around this value. The measurement of this resonance could be used to analyze back the speed of sound inside the slits.

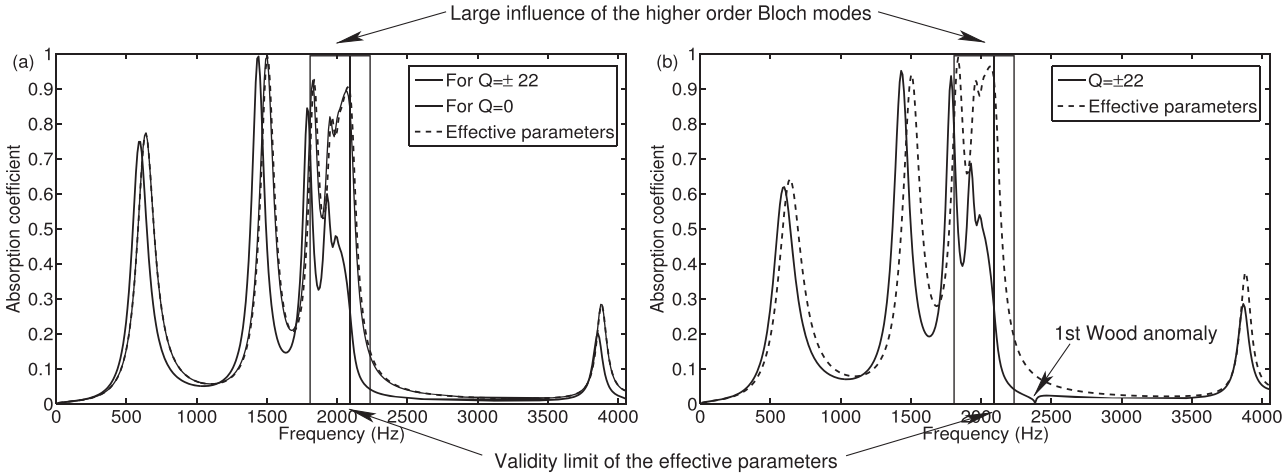

FIG. 5. Absorption coefficient for $L=42\,\text{mm}$, $N=2$, with $d^{(1)}=d^{(2)}=42\,\text{mm}$, with the quarter wavelength resonators plugged on the left for the first slit and on the right for the second slit, when $M=2$ and $Q^{\pm}=0$, $Q^{\pm}=22$ as well as the calculation ran with the equivalent parameters, (a) normal incidence, and (b) $\theta^i=\pi/4$.

Figure 5(b) depicts the absorption of the same configuration at $\theta^i=\pi/4$, when 3 modes are accounted for in the slits and $Q^{\pm}=22$ as well as the calculation ran with equivalent parameters derived in Sec. V. The bandgap frequency range and the position of the absorption peaks are identical, because the bandgap is due to quarter wavelength resonance of the tubes and because the large absorption peaks correspond to resonances of the slits. In practice, the calculation performed with the use of the effective parameters is in good agreement below the bandgap till grazing incidence despite the first Wood anomaly (which appears around 2100 Hz, Figure 5(b)).

The amplitude and frequency of the first absorption peak can further be improved with the help of the ratio $w/\phi^t l$, as explained in Sec. IV. This validates the previously effective parameters below the bandgap and proves the efficiency of the structure as sound absorbing metamaterial.

VII. EXPERIMENTAL VALIDATION

The samples were composed of an aluminum block of $40\times42\times42\,\text{mm}^3$. The block was drilled from side to side along the 40 mm thick direction with circular holes of $r=2.5\,\text{mm}$ equally spaced of 7 mm as shown Figure 5(a). This constitutes Sample 1. A 1 mm thick aluminum plate was then glued on one side of Sample 1 to close the holes. This constitutes Sample 2.

The absorption coefficient of the sample is measured in an impedance tube with a square cross section $4.2\,\text{cm}\times4.2\,\text{cm}$. The tube cut-off frequency is 4200 Hz. By assuming that plane waves propagate below the cut-off frequency, the infinitely rigid boundary conditions of the tube act like perfect mirrors and create a periodicity pattern in the x_1 and x_3 directions. Samples 1 and 2 are placed at the end of the tube against a copper plug that closes the tube and acts as a rigid boundary, therefore creating a periodicity along the x_1 direction of 8.4 cm with slit width $w=2\,\text{mm}$ and $w=1\,\text{mm}$, respectively, see Figure 5(a). This technique was previously used in various articles[10,23] and allows to determine experimentally the absorption coefficient at normal incidence of a quasi-infinite 2D periodic structure just with half or a quarter of the unit cell.

Figure 6(b) depicts the experimental absorption coefficient of Sample 1, the calculated one in the corresponding case, i.e., the one studied in Sec. VI and its approximation with the effective parameters. All the three curves match well below the bandgap. As explained in Sec. V, only the fully calculated absorption coefficient is valid inside the bandgap. Inside the latter, the experimental absorption coefficient is very low and is also difficult to measure, explaining the oscillations of the experimental curve. Figure 6(c) depicts the same curves for Sample 2, i.e., in the case $w=1\,\text{mm}$. Once again the curves match well. A small disagreement is noticed around f_l. This can be explained by several things related to the manufacturing and the misplacement of the sample, but more surely by the use of the impedance model. Effectively, the wavelength $(\text{Re}(c_2^s/f))$ is very small (while on the other hand the imaginary part $\text{Im}(c_2^s/f)$ is very large) and can be comparable to a around f_l, making improper the impedance model around this frequency. In both cases, the absorption for frequency higher than f_h is not well measured because the absorption is very low, but also because this frequency is very close from the cut-off frequency of the tube. These experiments were performed at two different levels of excitation, with identical results, ensuring the linearity of the response. These two experiments validate the previous method of calculation, as well as the derived effective parameters.

Of particular interest is the absorption coefficient of Sample 2, which exhibits a total absorption peak at 480 Hz, which corresponds to a wavelength in the air medium 17 times larger than the structure thickness.

VIII. CONCLUSION

The acoustic properties of a periodic arrangement of narrow irregularities (slits) with quarter-wavelength resonators plugged on it with a square lattice, whose periodicity is smaller than the wavelength is analyzed. It is shown that the wave propagating in the slit possesses the specific features of slow sound propagation over a quite large frequency band

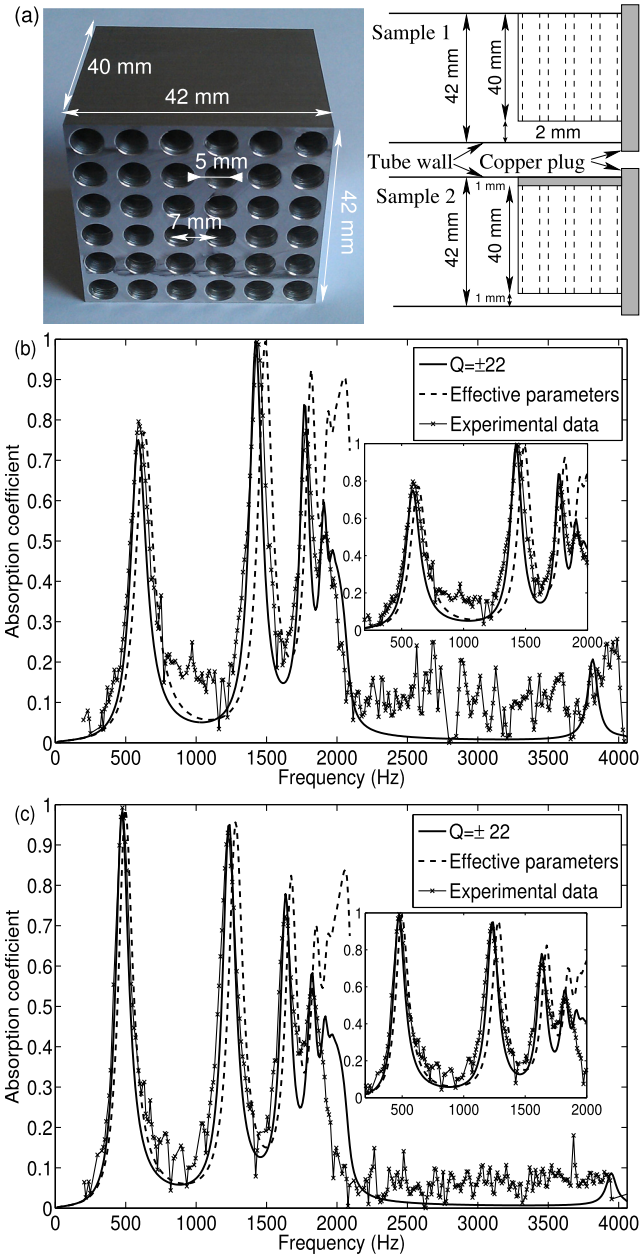

FIG. 6. Picture of Sample 1 (a), absorption coefficient of Sample 1 measured and simulated with the full model and with the effective parameters (b), and absorption coefficient of Sample 2 measured and simulated with the full model and with the effective parameters (c).

with a phase (and group) velocity much smaller than the one of air and the one of the wave propagating in the slit in absence of the quarter-wavelength resonators, for all frequencies below the resonance of the resonators. The associated dissipation is analyzed showing strong dependence with regards to the surface porosity, length of resonators, and width of the slit. The effective parameters are then derived, both for the modeling of the sound propagation in one slit, exhibiting negative bulk modulus inside the bandgap, and for the modeling of the whole structure, exhibiting in addition a unusual tortuosity effect. Of particular interest is the frequency limit of these effective parameters which are clearly identified, also pointing the interest of the use the Drude transition layers. These effective parameters also clearly show that the slow down of the sound speed in the slit is due to a modified bulk modulus together with an unusual tortuosity effect acting on the density of the slit. Both sound speed and dissipation are then used to design sound absorbing metamaterials, which exhibit a lowest frequency total absorption peak for wavelength much larger than four times the thickness of the structure. These results are validated experimentally, showing a lowest frequency total absorption peak for wavelength 17 times larger the thickness of the structure. This paves the way to the design of more complex sound absorbing structures, involving resonators of different nature, detuned resonators, and more complex arrangement.

ACKNOWLEDGMENTS

This work was partly supported by the ANR Project METAUDIBLE No. ANR-13-BS09-0003 co-founded by ANR and FRAE.

The authors would like to thank C. Boutin, B. Nennig, O. Umnova, and A. Merkel, for useful discussions on this work.

[1]L. Hau, S. Harris, Z. Dutton, and C. Behroozi, "Light speed reduction to 17 metres per second in an ultracold atomic gas," Nature **397**, 594–598 (1999).
[2]A. Santillan and S. Bozhevolnyi, "Demonstration of slow sound propagation and acoustic transparency with a serie of detuned resonators," Phys. Rev. B **89**, 184301 (2014).
[3]G. Yu and X. Wang, "Acoustical "transparency" induced by local resonance in bragg bandgaps," J. Appl. Phys. **115**, 044913 (2014).
[4]A. Cicek, O. Kaya, M. Yilmaz, and B. Ulug, "Slow sound propagation in a sonic crystal linear waveguide," J. Appl. Phys. **111**, 013522 (2012).
[5]Y. Aurégan, L. Xiong, and W. Bi, "Acoustical behavior of purely reacting liners," in *Proc. of 19th AIAA/CEAS Aeroacoustics Conference* (American Institute of Aeronautics and Astronautics, Inc., Berlin, 2013) pp. 1–8.
[6]W. Robertson, C. Baker, and C. Brad Bennet, "Slow group velocity propagation of sound via defect coupling in a one-dimensional acoustic band gap array," Am. J. Phys. **72**, 255–257 (2003).
[7]G. Theocharis, O. Richoux, V. Romero Garca, A. Merkel, and V. Tournat, "Limits of slow sound propagation and transparency in lossy, locally resonant periodic structures," New J. Phys. **16**, 093017 (2014).
[8]Z. Yang, J. Mei, M. Yang, N. Chan, and P. Sheng, "Membrane-type acoustic metamaterial with negative dynamic mass," Phys. Rev. Lett. **101**, 204301 (2008).
[9]J. Mei, G. Ma, M. Yang, Z. Yang, W. Wen, and P. Sheng, "Dark acoustic metamaterials as super absorbers for low-frequency sound," Nature Commun. **3**, 756 (2012).
[10]C. Lagarrigue, J.-P. Groby, V. Tournat, O. Dazel, and O. Umnova, "Absorption of sound by porous layers with embedded periodic array of resonant inclusions," J. Acoust. Soc. Am. **134**, 4670–4680 (2013).
[11]X. Olny and C. Boutin, "Acoustic wave propagation in double porosity media," J. Acoust. Soc. Am. **114**, 73–84 (2003).
[12]T. Dupont, P. Leclaire, O. Sicot, X. Gong, and R. Panneton, "Acoustic properties of air-saturated porous materials containing dead-end porosity," J. Appl. Phys. **110**, 094903 (2011).
[13]M. Stinson, "The propagation of plane sound waves in narrow and wide circular tubes, and generalization to uniform tubes of arbitrary cross-sectional shape," J. Acoust. Soc. Am. **89**, 550–558 (1991).
[14]C. Bradley, "Time harmonic acoustic bloch wave propagation in periodic waveguides. Part I. Theory," J. Acoust. Soc. Am. **96**, 1844–1853 (1994).
[15]E. Redon, A.-S. Bonnet-Ben Dhia, J.-F. Mercier, and S. Poernomo Sari, "Non-reflecting boundary conditions for acoustic propagation in ducts with acoustic treatment and mean flow," Int. J. Numer. Meth. Engng. **86**, 1360–1378 (2011).
[16]D. Muller, "A method for solving algebraic equations using an automatic computer," Math. Tables Aids Comput. **10**, 208–215 (1956).

[17]C. Boutin, "Acoustics of porous media with inner resonators," J. Acoust. Soc. Am. **134**, 4717–4729 (2013).
[18]N. Fang, D. Xi, J. Xu, M. Ambati, W. Srituravanich, C. Sun, and X. Zhang, "Ultrasonic metamaterials with negative modulus," Nature Mater. **5**, 452–456 (2006).
[19]P. Drude, "Transparent isotropic media," Wied. Ann **43**, 146 (1891).
[20]C. Simovski, "On electromagnetic characterization and homogenization of nanostructured metamaterials," J. Opt. **13**, 013001 (2011).
[21]J.-F. Allard and N. Atalla, *Propagation of Sound in Porous Media* (John Wiley & Sons, Ltd, Chichester, United-Kingdom, 2009), Chap. 4.
[22]J. Groby, A. Wirgin, L. De Ryck, W. Lauriks, R. Gilbert, and Y. Xu, "Acoustic response of a rigid-frame porous medium plate with a periodic set of inclusions," J. Acoust. Soc. Am. **126**, 685–693 (2009).
[23]J. Groby, W. Lauriks, and T. Vigran, "Total absorption peak by use of a rigid frame porous layer backed with a rigid multi-irregularities grating," J. Acoust. Soc. Am. **127**, 2865–2874 (2010).